Available online at www.sciencedirect.com
ScienceDirect
Trans. Nonferrous Met. Soc. China 27(2017) 1063−1070
Transactions of Nonferrous Metals Society of China
www.tnmsc.cn

Structure and oxidation resistance of $W_{1-x}Al_xN$ composite films

Xiao XIAO[1], Bei YAO[1,2]

1. School of Materials Science and Engineering, Tianjin University, Tianjin 300072, China;
2. Analysis Center, Tianjin University, Tianjin 300072, China

Received 25 March 2016; accepted 9 October 2016

Abstract: A series of $W_{1-x}Al_xN$ films ($0<x<38.6\%$, mole fraction) were deposited by reactive magnetron sputtering. The composition, microstructure, mechanical properties and oxidation resistance of the films were characterized by EPMA, XRD, XPS, nano-indentation, SEM and HRTEM. The effect of Al content on the microstructure and oxidation resistance of $W_{1-x}Al_xN$ films was investigated. The results show that WN film has a face-centered cubic structure. The preferred orientation changes from (111) to (200). The $W_{1-x}Al_xN$ films consist of a mixture of face-centered cubic W(Al)N and hexagonal wurtzite structure AlN phases. The hardness of the $W_{1-x}Al_xN$ films first increases and then decreases with the Al content increasing. The maximum hardness is 36 GPa, which is obtained at 32.4% Al (mole fraction). Compared with WN film, the $W_{1-x}Al_xN$ composite films show much better oxidation resistance because of the formation of dense Al_2O_3 oxide layer on the surface.

Key words: $W_{1-x}Al_xN$ film; microstructure; hardness; oxidation resistance; Al_2O_3 layer

1 Introduction

Hard thin films prepared by physical vapor deposition (PVD) are used to improve wear resistance of cutting tools undergoing tribological stress [1]. The first generation of PVD hard thin films (TiN, ZrN, CrN, etc.) has been widely used [2]. With the development of modern manufacturing, especially the appearance of dry and high speed machining, low friction coefficient, high hardness and low wear rate are demanded. Tungsten nitride thin film, as one of the first generation of thin films, has attracted growing attention due to its higher hardness, chemical stability, lower friction coefficient and better wear resistance at room temperature [3]. But it also shows poor oxidation resistance at high temperatures [4]. Since TiSiN composite films were prepared and studied [5], the researchers have observed that the poor oxidation resistance of binary films, at high temperatures, could be significantly improved with the incorporation of the elements which could improve the thermal stability [6−9], such as Al, Si and Y. Much work has been undertaken on the researches of ternary thin films (called them the second generation of hard thin films), such as CrAlN [10], TiSiN [11] and ZrAlN [12]. They showed improved properties like hardness as well as thermal stability and wear resistance at high temperature, due to the formation of an Al_2O_3 or SiO_2 oxide film on the surface. In this regard, the addition of aluminum into WN film is an effective way to improve its oxidation resistance. However, little attention has been paid to WAlN films.

The aim of this work was to prepare $W_{1-x}Al_xN$ films and investigate the structure, mechanical properties and oxidation resistance. $W_{1-x}Al_xN$ films with different Al contents were deposited by reactive magnetron sputtering. W_2N films were also produced for comparison purposes.

2 Experimental

$W_{1-x}Al_xN$ films, (2.1±0.1) μm thick (deposition time: 2 h), were deposited by radio frequency magnetron reactive sputtering on Si (100) wafer with a base pressure of 6.0×10^{-5} Pa. Water-cooled 75-mm-diameter W and Al targets with the same purity of 99.9%, were positioned at 78 mm from the substrate. The substrates were cleaned with successive rinses in ultrasonic baths of deionized water, alcohol and acetone and blown with dry air. High purity argon and nitrogen gases were introduced into the chamber from mass-flow controllers to reach a constant chamber pressure of 0.3 Pa. Just prior to initiating

Corresponding author: Bei YAO; Tel: +86-13389072752; E-mail: pyaotiju@163.com
DOI: 10.1016/S1003-6326(17)60124-9

deposition, the targets were sputter cleaned for 10 min while the substrate was covered with a protective shutter. Then, AlN film was deposited for 15 min to increase the adhesion, and the target power of Al was 100 W, at Ar/N_2 volume ratio of 10:3. During deposition, the substrates were continuously rotated about the polar axis with 50 r/min in order to obtain optimal coating uniformity. The target power of W was 120 W, the target power of Al was set to be 0, 60, 90, 120 and 150 W, respectively, with at Ar/N_2 volume ratio of 10:10. In order to investigate the oxidation resistance of the films, the samples were annealed at different temperatures (500, 600, 700, 800 °C) for 2 h in ambient atmosphere using the annealing oven. The samples were naturally cooled down to room temperature in the furnace before moving out for other analysis.

The composition of the samples was determined by an electron probe micro analyzer (EPMA). The crystal structures of as-deposited and annealed $W_{1-x}Al_xN$ films were investigated by X-ray diffraction (XRD) with a Cu K_α source, operated at 40 kV and 40 mA. The glancing incidence angle was 1° and the scanning speed was 4 (°)/min range of 30°−65°. The chemical bonds of the films were characterized by X-ray photoelectron spectroscopy (XPS) with Al K_α irradiation at a pass energy of 160 eV after removing the surface contaminants on the films by sputtering with Ar^+ ion beam at a primary energy of 3 keV for 3 min. The spectra were calibrated by the C 1s line with a binding energy of 284.5 eV, and then corrected for the linear emission background and decomposed into peaks with Gaussian−Lorentzian line shapes by a non-linear least-square fitting method. The surface morphologies before and after heat treatment were observed by scanning electron microscope (Nanosem 430). The microstructure was analyzed by a high resolution transmission electron microscope (HRTEM, field emission JEOL 2010F) operated at 200 kV. Hardness tests were conducted with a commercial nano-indentation hardness tester (Hysitro, Ti Premier), which equipped with a diamond Berkovich indenter tip (3-side pyramid). To ensure that the hardness was not influenced by the substrate, the maximum penetration depth of 100 nm which was always less than 10% of the coating thickness (2.0 μm) was used.

3 Results and discussion

3.1 Composition and microstructure

The composition of the $W_{1-x}Al_xN$ films as a function of Al target powers was determined by EPMA. The results are listed in Table 1. It is found that the Al content increases from 0 to 38.6% (mole fraction) with increasing the Al target power from 0 to 150 W, however, the W content appears to decrease gradually. The hardness values of the $W_{1-x}Al_xN$ films are also listed in Table 1. As shown in Table 1, the hardness gradually increases from 28 GPa for pure WN film to 36 GPa for the film containing 32.4% Al. As the Al content increases to 38.6%, the hardness decreases to 35 GPa.

Table 1 Chemical composition, hardness and average grain size of $W_{1-x}Al_xN$ composite films

Power of Al target/W	Mole fraction/%		Film thickness/μm	Hardness/GPa	Average grain size/nm
	W	Al			
0	100	0	2	28	16.8±1.7
60	87.6	12.4	2.1	30	16.0±1.4
90	78.0	22.0	2.1	33	14.1±1.0
120	67.6	32.4	2.1	36	12.9±0.7
150	61.4	38.6	2.2	35	13.7±0.3

The XRD patterns of $W_{1-x}Al_xN$ films with different Al contents are presented in Fig. 1. As shown, WN film has a δ-NaCl FCC-structure with the (111) and (200) preferred orientation (PDF card No. 25−1257), which is corresponding to WN phase. $W_{1-x}Al_xN$ films share a similar structure regardless of Al content. With the increase of Al content, the (111) diffraction peak of the $W_{1-x}Al_xN$ films becomes weaker and the (200) diffraction peak shifts toward higher diffraction angles, indicating a decrease in the lattice parameter.

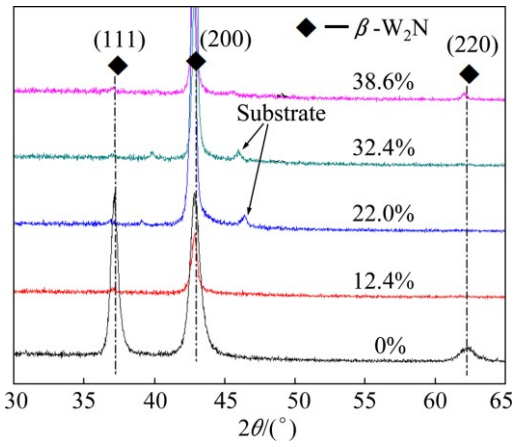

Fig. 1 XRD patterns of $W_{1-x}Al_xN$ composite films with different Al contents

According to the Bragg equation [13], the lattice parameters (a) of $W_{1-x}Al_xN$ films with different Al contents were calculated. The results are shown in Fig. 2. As shown in Fig. 2, the incorporation of Al results in a decrease of the lattice parameter. This is probably due to the fact that the W atoms (atomic radius: 0.139 nm) are substituted by Al atoms (atomic radius: 0.125 nm) during the preparation of $W_{1-x}Al_xN$ films. With the increase of

Al content, more W atoms are substituted. This results in a further decrease of lattice parameters of $W_{1-x}Al_xN$. No XRD signals corresponding to AlN phase are found.

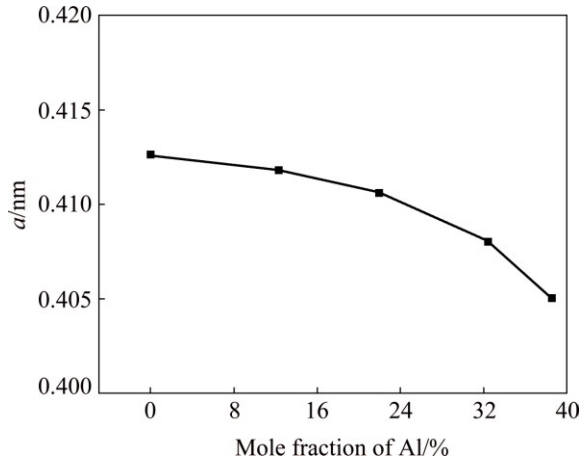

Fig. 2 Lattice constants of $W_{1-x}Al_xN$ composite films with different Al contents

In order to study the bonding state of $W_{1-x}Al_xN$ films, XPS analysis was carried out. The XPS analysis results are shown in Fig. 3. As shown in Fig. 3, two peaks are found at 73.0 and 74.6 eV, which are ascribed to W(Al)—N and Al—N bonds, respectively [14,15]. With the increase of Al content, the peak intensity of W(Al)—N decreases coupling with the increase of the peak intensity of Al—N. This suggests that the amount of AlN increases and the amount of W(Al)N decreases.

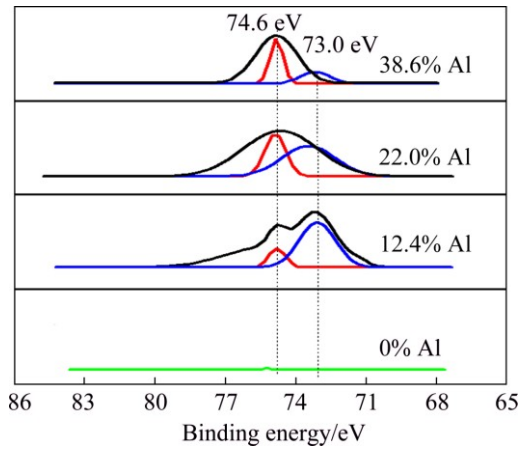

Fig. 3 XPS analysis of Al 2p photoelectron spectra of $W_{1-x}Al_xN$ films

The HRTEM images of the WN and $W_{0.78}Al_{0.22}N$ films are shown in Fig. 4. As shown in Fig. 4(a), for WN film, two lattice fringes are observed and the lattice spacing values are 0.238 and 0.206 nm, respectively. For WN film, the values of (111) and (200) lattice spacing are 0.24 and 0.208 nm in JCPDS data. This suggests that the calculated values are nearly in agreement with the theoretical values. As shown in Fig. 4(b), for $W_{0.78}Al_{0.22}N$ film, two lattice fringes are also observed and the lattice spacing values are 0.236 and 0.210 nm, respectively. According to the reported studies [14−16], these values of the lattice fringes are nearly consistent with the values of HCP-AlN (101) and FCC-W_2N (200) in JCPDS data. According to the above analysis, the films consist of a mixture of FCC-W(Al)N and HCP-AlN phases.

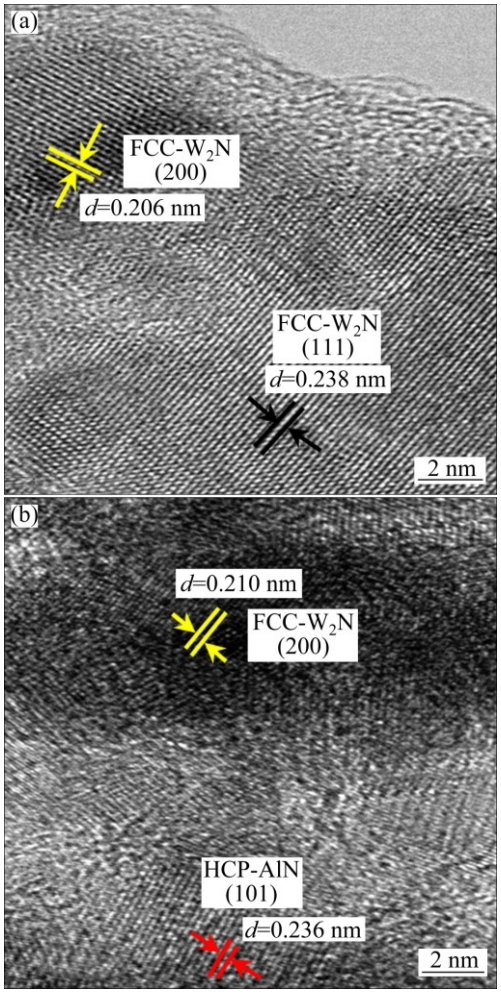

Fig. 4 HRTEM images of different films: (a) WN film; (b) $W_{0.78}Al_{0.22}N$ film

The crystalline sizes of $W_{1-x}Al_xN$ composite films were calculated utilizing Scherre's equation [13]. The results are also listed in Table 1. As listed, the average grain size of WN is 16.8 nm. As the Al content increases, the grain size first decreases gradually and then increases. A minimum value of 12.9 nm is obtained as the Al content is 32.4%.

3.2 Oxidation resistance

Figure 5 shows the XRD patterns of $W_{1-x}Al_xN$ films after annealing at different temperatures for 2 h. As shown in Fig. 5(a), after oxidation at 500 °C, WO_3 diffraction peaks are only detected on the surface of WN

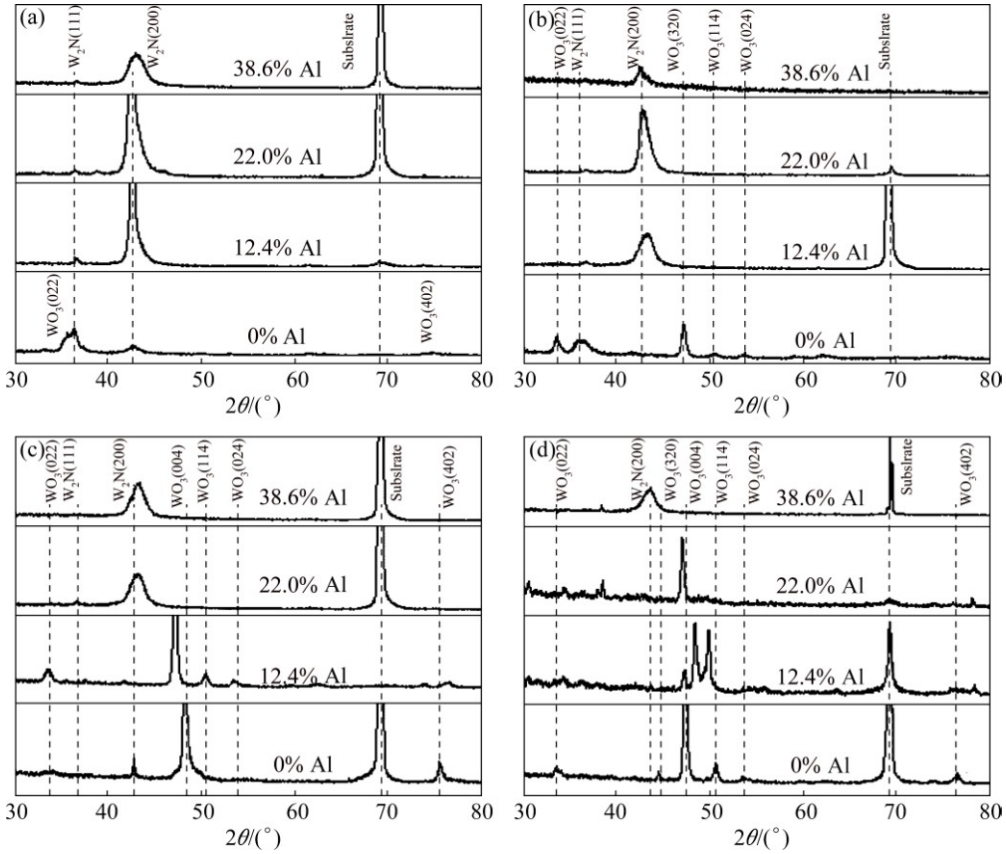

Fig. 5 XRD patterns of $W_{1-x}Al_xN$ composite films at different annealing temperatures: (a) 500 °C; (b) 600 °C; (c) 700 °C; (d) 800 °C

film. This suggests that the films containing Al content are not oxidized after oxidation at 500 °C for 2 h. As shown in Fig. 5(b), after oxidation at 600 °C, the intensities of WO_3 diffraction peaks detected on the surface of WN film become stronger, while no evident oxide peaks are detected in $W_{1-x}Al_xN$ films. This indicates that the oxidation degree of WN film increases but the $W_{1-x}Al_xN$ films still maintain a good oxidation resistance. Figure 5(c) shows that, when the annealing temperature increases up to 700 °C, some WO_3 peaks could be observed on the surface of the $W_{0.876}Al_{0.124}N$ film. However, no diffraction peaks corresponding to oxides are detected on the surface of $W_{1-x}Al_xN$ films (x>12.4%), indicating that the $W_{1-x}Al_xN$ films with more than 12.4% Al still keep a good oxidation resistance. Figure 5(d) illustrates that the $W_{0.614}Al_{0.386}N$ composite film can maintain good oxidation resistance after annealing at 800 °C, because no WO_3 peaks are detected on the surface of $W_{0.614}Al_{0.386}N$ film. According to Fig. 5, the oxidation resistance of WN film is improved by adding the aluminum element.

Figure 6 illustrates the W 4f and Al 2p spectra of the $W_{0.676}Al_{0.324}N$ film after oxidation at 700 °C for 2 h. As shown in Fig. 6(a), two contributions are found at 34 and 36 eV, which are ascribed to W(Al)—N and W—O bonds, respectively [17]. This can be assigned to WAlN and WO_3, respectively. Similarly, the Al 2p spectrum can be deconvolved into two subpeaks, centered at about 73.0 and 75.3 eV, which can be assigned to WAlN and Al_2O_3 [17,18], respectively. The XPS results demonstrate that the surface of $W_{0.676}Al_{0.324}N$ film is only partially oxidized.

The SEM images of $W_{0.676}Al_{0.324}N$ films oxidized at different temperatures are presented in Fig. 7. As shown in Fig. 7, the oxidized surface of films still maintains dense pebble-like structure with uniform grains at temperatures below 600 °C. As the oxidation temperature increases to 700 °C, some micropores and upheavals can be observed to distribute among the grain boundaries. This could speed up the diffusion of oxygen to promote the oxidation of films. As the oxidation temperature further increases to 800 °C, some cracks are found on the surface, which makes it easy to promote the inward diffusion of oxygen. According to Ref. [19], volume expansion generated by the oxide reaction and phase transformation should result in the formation of microcracks. The bulk densities of WAlN, WO_3 and Al_2O_3 are 16.2, 7.16 and 3.99 g/cm^3, respectively. The bulk densities of the films decrease after oxidation. This would result in an enormous volume expansion. At 700 °C, the difference of the bulk densities resulted from the formation of WO_3 and Al_2O_3 is just enough to

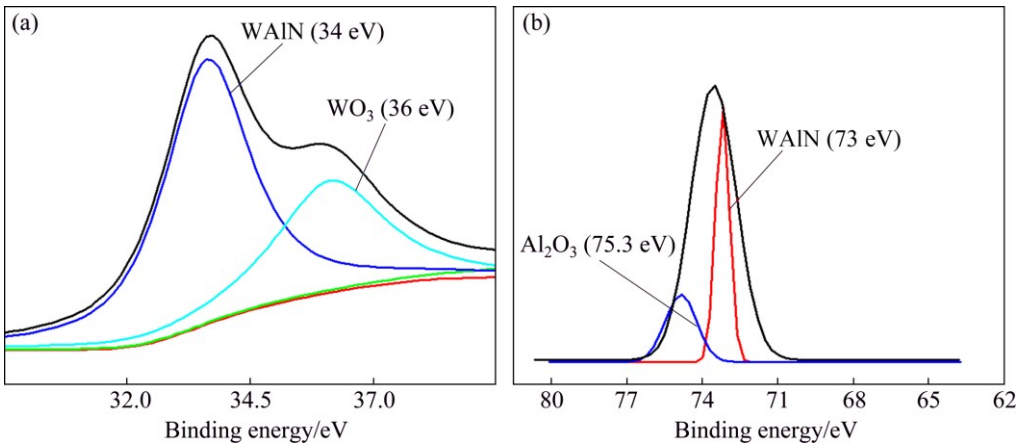

Fig. 6 XPS spectra of $W_{0.676}Al_{0.324}N$ film after oxidation at 700 °C for 2 h: (a) W 4f spectra; (b) Al 2p spectra

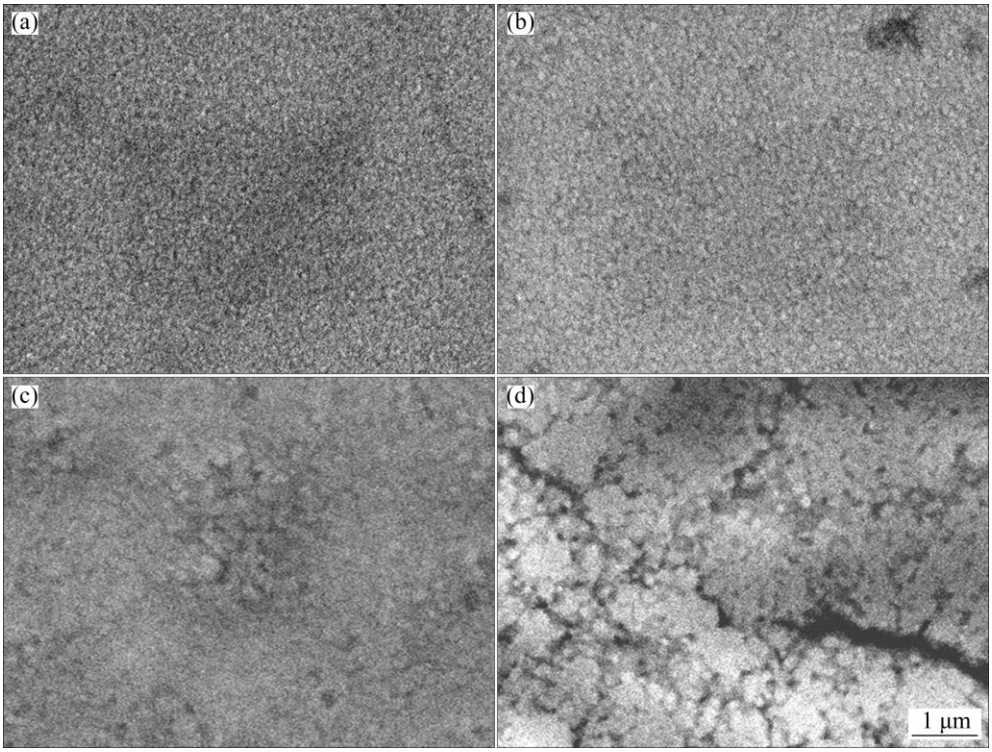

Fig. 7 SEM images of $W_{0.676}Al_{0.324}N$ film oxidized at different temperatures: (a) 500 °C; (b) 600 °C; (c) 700 °C; (d) 800 °C

produce some pores and upheavals. At 800 °C, the difference of the bulk densities resulted from the formation of WO_3 and Al_2O_3 could produce cracks.

Figure 8 illustrates the changing curve of Al content on the surface of $W_{0.676}Al_{0.324}N$ film oxidized at different temperatures. As shown in Fig. 8, with the temperature increasing, the relative content of Al on the oxidized surface increases gradually. During the high-temperature oxidation, it is interesting to note that Al_2O_3 is formed more easily than WO_3, because the Gibbs free energies for Al_2O_3 and WO_3 are −1456.1 and −764 kJ/mol, respectively. For this reason, the Al atoms would diffuse to the film surface to bond with O atoms. Thus, the relative content of Al on the film surface increases slightly.

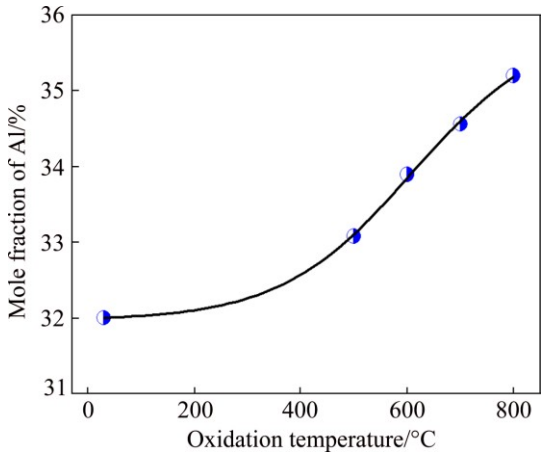

Fig. 8 Al content on surface of $W_{0.676}Al_{0.324}N$ film oxidized at different temperatures

The SEM images of surface and fracture morphologies of WN, $W_{0.876}Al_{0.124}N$ and $W_{0.676}Al_{0.324}N$ films, after oxidation at 700 °C for 2 h, are shown in Fig. 9. Some cracks are observed on the oxidized surface of Al-free WN film. This is because the larger difference in the bulk densities of WAlN and WO_3 according to the above analysis. Numbers of micropores are found on the oxidized surface of $W_{0.876}Al_{0.124}N$ film, because of the difference in the bulk densities of WAlN, WO_3 and Al_2O_3. Some upheavals are found on the surface of $W_{0.676}Al_{0.324}N$ film. This is also attributed to the difference in the bulk densities of WAlN, WO_3 and Al_2O_3. All the films exhibit dense and adherent oxide scale (marked by red lines), which share a columnar structure. The formation of oxide scale with thickness of ~0.9 μm is found for Al-free WN film. With further increasing Al content to 12.4%, the thickness of the oxide scale decreases to ~0.6 μm. As the Al content reaches 32.4%, the thickness of the oxide scale further decreases to ~0.3 μm.

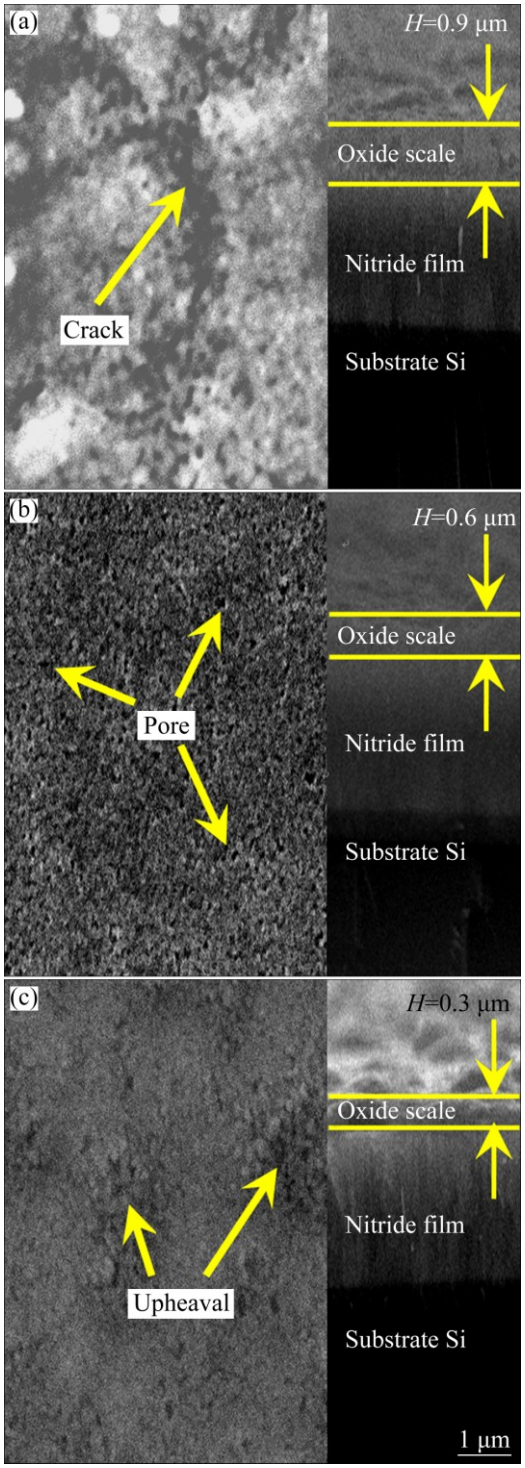

Fig. 9 SEM images of surface and fracture morphologies of different films oxidized at 700 °C for 2 h: (a) WN film; (b) $W_{0.876}Al_{0.124}N$ film; (c) $W_{0.676}Al_{0.324}N$ film

An analytical TEM study was performed to investigate the structural insight into the oxide scale of the $W_{1-x}Al_xN$ films. Figure 10 shows the fracture image of the $W_{0.676}Al_{0.324}N$ film after oxidation at 700 °C for 2 h and the corresponding HRTEM images of zones *A*, *B* and *C*. As shown in zone *A*, a lattice fringe with a lattice spacing of about 0.21 nm is observed. This value is nearly consistent with that shown in JCPDS data, where the value of (402) lattice spacing for α-Al_2O_3 is 0.209 nm. In other words, this lattice fringe is corresponding to the α-Al_2O_3 (402). Similarly, WO_3 is observed in zone *B* and only W_2N exists in zone *C*. Thus, the oxide scale consists of an Al_2O_3 outer layer (zone *A*) and a WO_3 inner layer (zone *B*).

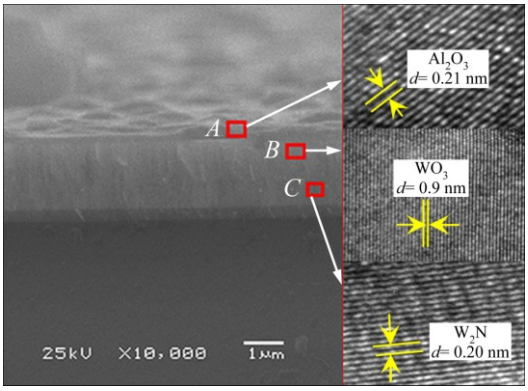

Fig. 10 Fracture image of $W_{0.676}Al_{0.324}N$ film oxidized at 700 °C for 2 h and corresponding HRTEM images: zone *A* for top layer; zone *B* for interlayer; zone *C* for bottom layer

It can be learned from the above analyses that the addition of aluminum can improve the oxidation resistance of WN films. This can be considered as follows. Firstly, the added Al atoms replace the situation of W atoms to form FCC-W(Al)N structure, which results in the metallic bonding (W—N) transferring to covalent bonds (Al—N). The increase in bonding energy could improve the thermal stability and inhibit the decomposition of FCC-W(Al)N. Secondly, the W^{6+} and Al^{3+} combine with the oxygen by diffusing outward the

film surface to form the mixture oxide scale of Al_2O_3 and WO_3. These oxide layers with dense structure can act as an effective diffusion barrier to slow down the inward diffusion of oxygen at high temperatures and increase the oxidation resistance of $W_{1-x}Al_xN$ films.

4 Conclusions

1) WAlN films consist of a mixture of face-centered cubic W(Al)N and hexagonal wurtzite structure AlN phases. With the increase of Al content, the lattice parameters decrease gradually, while the grain size and hardness decrease first and then increase.

2) The surface morphologies have obvious change for the films oxidized at different temperatures due to the difference of the bulk densities of WAlN, WO_3 and Al_2O_3. For $W_{0.676}Al_{0.324}N$ film, the oxidized surface still maintains dense pebble-like structure with uniform grains at temperatures below 600 °C; some micropores and upheavals distributing among the grain boundaries can be observed at 700 °C; some cracks are found on the surface at 800 °C.

3) The oxidation resistance of WN film is improved by adding the aluminum element. All the films exhibit dense and adherent oxide scale, which share a columnar structure. The oxide scale consists of an Al_2O_3 outer layer and a WO_3 inner layer.

References

[1] ERDEMIR A. A crystal chemical approach to the formulation of self-lubricating nanocomposite coatings [J]. Surface and Coatings Technology, 2005, 200(5): 1792−1796.

[2] SHAN Lei, ZHANG Yang-rong, WANG Yong-xin, LI Jin-long, JIANG Xin, CHEN Jian-min. Corrosion and wear behaviors of PVD CrN and CrSiN coatings in seawater [J]. Transactions of Nonferrous Metals Society of China, 2016, 26(1): 175−184.

[3] ZHAO Hong-jian, NI Zeng-lei, YE Fu-xing. Effect of carbon content on structure and properties of WCN coatings prepared by RF magnetron sputtering [J]. Surface and Coatings Technology, 2016, 287: 129−137.

[4] GASSNER G, MAYRHOFER P H, KUTSCHEJ K, MITTERER C, KATHREINC M. Magnéli phase formation of PVD Mo−N and W−N coatings [J]. Surface and Coatings Technology, 2006, 201(6): 3335−3341.

[5] KIM K H, PARK B H. Mechanical properties and oxidation behavior of Ti−Si−N films prepared by plasma-assisted CVD [J]. Chemical Vapor Deposition, 1999, 5(6): 275−279.

[6] WANG Tao, ZHANG Guo-jun, LIU Zhuan-ning, JIANG Bai-ling. Oxidation behavior of magnetron sputtered Mo_2N/AlN multilayer coatings during heat treatment [J]. Ceramics International, 2015, 41(5): 7028−7035.

[7] LIN J, MISHRA B, MOORE J J, SPROUL W D. A study of the oxidation behavior of CrN and CrAlN thin films in air using DSC and TGA analyses [J]. Surface and Coatings Technology, 2008, 202(14): 3272−3283.

[8] HSIEH J H, TAN A L K, ZENG X T. Oxidation and wear behaviors of Ti-based thin films [J]. Surface and Coatings Technology, 2006, 201(7): 4094−4098.

[9] DING Xing-zhao, ZENG Xian-ting. Structural, mechanical and tribological properties of CrAlN coatings deposited by reactive unbalanced magnetron sputtering [J]. Surface and Coatings Technology, 2005, 200(5): 1372−1376.

[10] SCHALK N, WEIRATHER T, SABITZER C, HIRN S, V. L. TERZIYSKA V L, GANGOPADHYAY S, CZETTL C, POLCIK P, KATHREIN M, MITTERER C. Combinatorial synthesis of $Cr_{1-x}Al_xN$ and $Ta_{1-x}Al_xN$ coatings using industrial scale co-sputtering [J]. Surface Engineering, 2016, 32(4): 252−257.

[11] CHENG Y H, BROWNE T, HECKERMAN B, MELETIS E I. Mechanical and tribological properties of nanocomposite TiSiN coatings [J]. Surface and Coatings Technology, 2010, 204(14): 2123−2129.

[12] LI De-jun. Synthesis of ZrAlN coatings with thermal stability at high temperature [J]. Science in China (Series E): Technological Sciences, 2006, 49(5): 576−581.

[13] YU Li-hua, ZHAO Hong-jian, XU Jun-hua. Mechanical, tribological and corrosion performance of WBN composite films deposited by reactive magnetron sputtering [J]. Applied Surface Science, 2014, 315: 380−386.

[14] YANG Jun-feng, JIANG Yan, YUAN Zhi-gang, WANG Xian-ping, FANG Qian-feng. Effect of carbon content on the microstructure and properties of WSiCN coatings fabricated by magnetron sputtering [J]. Materials Science and Engineering B, 2012, 177(13): 1120−1125.

[15] SUBRAMANIAN B, SWAMINATHAN V, JAYACHANDRAN M. Micro-structural and optical properties of reactive magnetron sputtered aluminum nitride (AlN) nanostructured films [J]. Current Applied Physics, 2011, 11(1): 43−49.

[16] HUGOSSON H W, HOGBERG H, ALGREN M, RODMAR M, SELINDER T I. Theory of the effects of substitutions on the phase stabilities of $Ti_{1-x}Al_xN$ [J]. Journal of Applied Physics, 2003, 93(8): 4505−4511.

[17] ZHAO Hong-jian, YE Fu-xing. Effect of Si-incorporation on the structure, mechanical, tribological and corrosion properties of WSiN coating [J]. Applied Surface Science, 2015, 356: 958−966.

[18] WANG Rui, LI Jing-long, WANG Yong-xin, HU Jian-min, WU Hai-zhong. High temperature oxidation behavior and mechanical properties of TiAlN/SiN decorative films on borosilicate glass by magnetron sputtering [J]. Thin Solid Films, 2015, 584: 72−77.

[19] WU Zheng-tao, QI Zheng-bing, ZHANG Dong-fang, WANG Zhou-cheng. Evolution of the microstructure and oxidation resistance in co-sputtered Zr−Y−N coatings [J]. Applied Surface Science, 2014, 321: 268−274.

$W_{1-x}Al_xN$ 复合膜的显微组织和抗氧化性能

肖 晓[1]，姚 琲[1,2]

1. 天津大学 材料科学与工程学院，天津 300072；2. 天津大学 分析中心，天津 300072

摘 要：采用反应磁控溅射仪制备一系列不同铝含量(0~38.6%，摩尔分数)的 $W_{1-x}Al_xN$ 复合膜。利用 EPMA、XRD、XPS、纳米压痕仪、SEM 及 HRTEM 等对膜组成、显微组织、力学及抗氧化性能进行表征，研究 Al 含量对 WAlN 膜显微组织和抗氧化性能的影响。结果表明，WN 膜为面心立方结构，$W_{1-x}Al_xN$ 膜由面心立方 W(Al)N 和六方纤锌矿结构 AlN 组成，具有很强的(111)和(200)取向。其硬度随 Al 含量增加先增大后减小。当 Al 含量为 32.4%(摩尔分数)时硬度达到最大值，为 36 GPa。与 WN 相比，$W_{1-x}Al_xN$ 膜表现出更优的抗氧化性能，这主要归因于表层形成的致密 Al_2O_3 层。

关键词：$W_{1-x}Al_xN$ 膜；显微组织；硬度；抗氧化性能；Al_2O_3 层

(Edited by Wei-ping CHEN)